Precursor design for efficient synthesis of large-pore, sulfur-doped ordered mesoporous carbon through direct pyrolysis

Journal:	*Molecular Systems Design & Engineering*
Manuscript ID	ME-ART-03-2023-000043.R1
Article Type:	Paper
Date Submitted by the Author:	05-May-2023

Complete List of Authors:	Robertson, Mark; University of Southern Mississippi, School of Polymer Science and Engineering Griffin, Anthony; University of Southern Mississippi, School of Polymer Science and Engineering Guillen Obando, Alejandro; The University of Southern Mississippi, School of Polymer Science and Engineering Barbour, Andrew; University of Southern Mississippi, School of Polymer Science and Engineering Davis, Ryan; University of Southern Mississippi, School of Polymer Science and Engineering Qiang, Zhe; University of Southern Mississippi, School of Polymer Science and Engineering

Design, System, and Application

Generally, synthetic methods for the production of ordered mesoporous carbons (OMCs) through direct pyrolysis of block copolymers involve several sophisticated steps for precursor preparation and long crosslinking times, which can result in the entire manufacuting process being high-cost and time-consuming. In this work, we address these challenges by demonstrating an efficient OMC precursor platform and system design with rapid crosslinking kinetics and controlled ordered structures. Specifically, through using polystyrene-block-polybutadiene-block-polystyrene, which contains unsaturated groups in the polymer backbone, sulfonation-induced crosslinking reaction can be accomplished with much faster kinetics than most conventional systems. Upon carbonization, these materials can produce OMCs with large mesopores and sulfur-doped frameworks. These desired features can enable enhanced diffusion and sorption of large-size molecules within OMC pore channels, which are particularly attractive for many applications such as drug delivery and water remediation. The reported system can complement with soft-templating methods for OMC synthesis, which typically yield small mesopores (e.g. < 6 nm) from the cooperative assembly of phenolic resin and commerical surfactant templates.

ARTICLE

Precursor design for efficient synthesis of large-pore, sulfur-doped ordered mesoporous carbon through direct pyrolysis

Received 00th January 20xx,
Accepted 00th January 20xx

DOI: 10.1039/x0xx00000x

Mark Robertson,[a] Anthony Griffin, [a] Alejandro Guillen Obando, [a] Andrew Barbour, [a] Ryan Davis, [a] and Zhe Qiang [a, *]

The production of ordered mesoporous carbons (OMCs) can be achieved by direct pyrolysis of self-assembled polymers. Typically, these systems require a majority phase capable of producing carbon, and a minority phase to form pores through a thermal decomposition step. While polyacrylonitrile (PAN)-based block copolymers (BCPs) have been broadly reported as OMC precursors, these materials have a relatively narrow processing window for developing ordered nanostructures and often require sophisticated chemistry for BCP synthesis, followed by long crosslinking times at high temperatures. Alternatively, olefinic thermoplastic elastomers (TPEs) can be convered to large-pore OMCs after two steps of sulfonation-induced crosslinking and carbonization. Building on this platform, this work focuses on the precursor design concept for the efficient synthesis of OMCs through employing low-cost and widely available polystyrene-*block*-polybutadiene-*block*-polystyrene (SBS), which contains unsaturated bonds along the polymer backbone. As a result, the prescence of alkene groups greatly enhances the kinetics of sulfonation-induced crosslinking reaction, which can be completed within only 20 min at 150 °C, nearly an order of magnitude faster than a recently reported TPE system containing a fully saturated polymer backbone. The crosslinking reaction enables the production of OMCs with pore sizes (~9.5 nm) larger than most conventional soft-templating systems, while also doping sulfur heteroatoms into the carbon framework of the final products. This work demonstrates efficient synthesis of OMCs from TPE precursors which have a great potential for scaled production, and the resulting products may have broad applications such as for drug delivery and energy storage.

Design, System, and Application

Generally, synthetic methods for the production of ordered mesoporous carbons (OMCs) through direct pyrolysis of block copolymers involve several sophisticated steps for precursor preparation and long crosslinking times, which can result in the entire manufacuturing process being high-cost and time-consuming. In this work, we address these challenges by demonstrating an efficient OMC precursor platform and system design with rapid crosslinking kinetics and controlled ordered structures. Specifically, through using polystyrene-*block*-polybutadiene-*block*-polystyrene, which contains unsaturated groups in the polymer backbone, sulfonation-induced crosslinking reaction can be accomplished with much faster kinetics than most conventional systems. Upon carbonization, these materials can produce OMCs with large mesopores and sulfur-doped frameworks. These desired features can enable enhanced diffusion and sorption of large-size molecules within OMC pore channels, which are particularly attractive for many applications such as drug delivery and water remediation. The reported system can complement with soft-templating methods for OMC synthesis, which typically yield small mesopores (e.g. < 6 nm) from the cooperative assembly of phenolic resin and commerical surfactant templates.

Introduction

Porous carbons are extensively used in various applications due to the combination of carbon properties (e.g. chemical inertness, electrical and thermal conductivity, mechanical stability) and porosity which facilitates interactions between guest molecules and the carbon matrix.[1–3] Ordered mesoporous carbons (OMCs) represent a subclass of porous carbons which contain uniform structures with pore sizes in the range from 2 to 50 nm.[4] The immense utility of OMCs has been demonstrated in a variety of fields including energy storage,[5,6] water remediation,[7,8] gas capture,[9] biomedicine,[10,11] and catalysis.[12] In general, OMCs synthesis have been relied on the self-assembly of polymeric materials to form ordered mesostructures. For instance, conventional soft-templating route employs evaporation induced self-assembly of amphiphilic polymers/surfactants and phenolic resin (resol), which act as templating agents and carbon precursors, respectively.[13,14] Upon the evaporation of solvent, resol can cooperatively assemble into well-ordered nanodomains, which can then be crosslinked and carbonized. While the soft-templating method

[a] *School of Polymer Science and Engineering, University of Southern Mississippi, Hattiesburg, MS, 39406*

Electronic Supplementary Information (ESI) available: Differential scanning calorimetry thermogram and supplemental nitrogen physisorption isotherms/pore size distributions. See DOI: 10.1039/x0xx00000x

can effectively access a variety of pore textures, it involves large-scale solvent consumption and several time-consuming steps. For example, steps of solvent evaporation and resol crosslinking would respectively require at least a few hours.[15] Additionally, the attainable pore sizes from soft-templating methods using commercially available templating agents (e.g. surfactant molecules) are generally restricted up to 6 nm.

An alternative method for OMC synthesis is through the direct pyrolysis of block copolymers (BCPs). In these systems, the ability of BCP self-assembly to establish well-ordered nanostructures is leveraged through synthesizing precursors which contain a majority phase that can be converted to carbon, while the minority domains can be decomposed to form pores. In previous works, direct pyrolysis of BCPs generally relies on precursors which contain polyacrylonitrile (PAN) as the majority phase of the material.[16–18] PAN undergoes a self-crosslinking reaction simply through the application of heat which allows it to produce a carbon matrix after exposure to high temperatures in an inert atmosphere.[15] PAN-derived precursors are advantageous because they provide inherently nitrogen-doped carbons which can enhance their utility in many applications.[19,20] Through direct pyrolysis of BCP precursors, the resulting pore sizes are often much larger than conventional surfactant-templated OMCs. Notably, as highlighted in several review and perspective articles, large-pore OMCs are highly desired for separation, sorption, loading, and transport of large molecules such as proteins, viruses, as well as nanoparticles.[21–23] However, one challenge in PAN-based materials is that they typically have a limited processing window for developing ordered nanostructures, due to the high glass transition and melting temperatures of PAN segment, while the PAN crosslinking reaction can occur starting around 200 °C.[24,25] As a result, it might be challenging to achieve long-range ordering in PAN-based BCPs, as well as their derived OMCs.[18]

The application of thermoplastic elastomers (TPEs) as a new type of OMC precursor through direct pyrolysis approach has been very recently reported, providing an exciting new avenue to synthesize OMC using low-cost and widely available chemicals.[26] Generally, TPE-based BCPs contain a polyolefin majority phase and some high glass transition temperature (T_g) minority components, such as polystyrene. These materials can spontaneously form ordered nanostructures, where assembled glassy domains can serve as physical crosslinkers.[27] A sulfonation-induced crosslinking reaction was employed to selectively crosslink the polyolefin majority phase of a polystyrene-*block*-poly(ethylene-*ran*-butylene-*block*-polystyrene) (SEBS) block copolymer, allowing it to be successfully converted into a carbon matrix while the polystyrene (and their derived sulfonated products) minority phases can be decomposed to form pores. The OMCs fabricated through this process can exhibit improved degree of ordering in comparison to PAN-based precursors, pore sizes larger than 10 nm, as well as sulfur-doped carbon frameworks. While the sulfonation-crosslinking method was generalizable to multiple different SEBS precursors for OMC synthesis, these systems still require at least a few hours to accomplish crosslinking. With a vision toward scale-up and efficient energy use, it would be ideal to enable faster reaction kinetics through rational precursor and/or system design. A previous work explored the opportunity of employing SIS as porous carbon precursor, however, the polyisoprene segment was highly reactive, and the rigorous sulfonation reaction led to completely disordered nanostructures after the crosslinking step.[28]

In this work, we report how the design of TPE precursors and engineering of the fabrication process can improve the synthesis of OMCs, including significantly accelerated sulfonation-crosslinking reaction kinetics and improved degree of ordering. Specifically, polystyrene-*block*-polybutadiene-*block*-polystyrene (SBS) is used as a nanostructured precursor. The presence of unsaturated bonds within the polybutadiene (PB) majority phase greatly enhances the crosslinking kinetics (nearly an order of magnitude) in comparison to SEBS-based precursors, enabling completed crosslinking within 20 min at 150 °C. Additionally, the impact of reaction conditions (e.g. time and temperature) on the morphology development and chemical compositions of the final OMC products is systematically investigated, allowing informed process design for manufacturing SBS-derived OMC materials.

Experimental Section

Materials

Poly(styrene)-*block*-poly(butadiene)-*block*-poly(styrene) (SBS; M_n: 140,000 g/mol, ϕ_{PS} = 0.33, Đ = 1.15), toluene (>99.5%) and sulfuric acid (98%) were obtained from Sigma Aldrich. A Millipore Sigma Milli-Q IQ 7003 ultrapure lab water purification system was used to obtain deionized (DI) water.

Synthesis of SBS-derived OMC

To prepare SBS-derived OMC, 1 g of SBS (pellets form, averaged diameter of ~4 mm) was placed in a reaction vessel containing 3g of sulfuric acid, which was then heated at 100 °C or 150 °C for varying amounts of time. Following sulfonation, the crosslinked sample was removed and washed with DI water three times to remove byproducts and residual acid. Subsequently, the samples were then dried overnight at 125 °C and carbonized under a N_2 atmosphere at a rate of 1 °C/min to 600 °C and thereafter 5 °C/min to 800 °C using an MTI Corporation OTF-1200× tube furnace. As a note, carbonization process may produce various SO_x gaseous products and care should be taken to ensure that they are properly ventilated.

Characterization

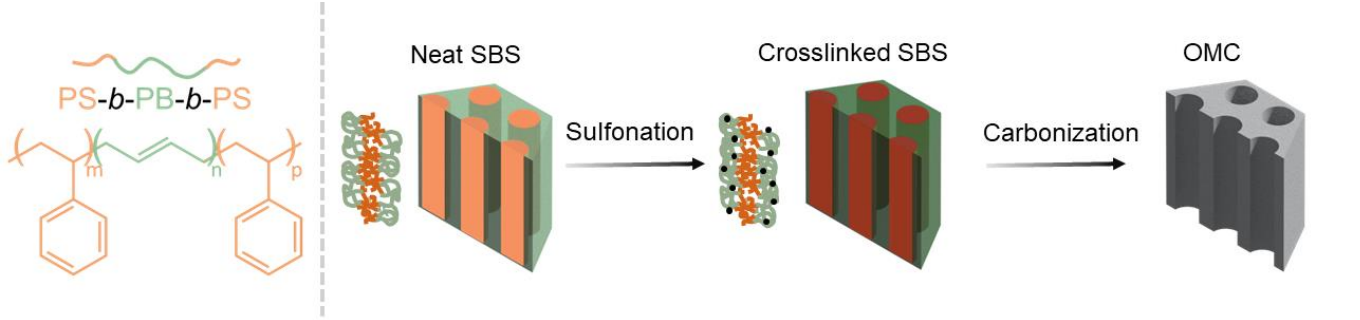

Figure 1. Representative chemical structure of SBS and a schematic illustration of the sulfonation process used to convert the cylinder forming BCPs to OMCs. As a note, the chemical structure of poly(1,4-butadiene) (PB) segment is simplified, as other isomers may exist.

Chemical compositions of SBS and derived sulfonated samples were characterized using a Frontier attenuated total reflection Fourier transform infrared (FTIR) spectrometer (PerkinElmer). Spectra were collected at a wavenumber range of 4000-600 cm^{-1} with an average of 32 scans at a resolution of 4 cm^{-1}. Mass gain was calculated by comparing the mass of the sulfonated sample to the mass of the sample before reaction, and gel fractions were determined by vigorously stirring the sulfonated materials in toluene for 1 h to remove any un-crosslinked material. The mass of the sample after extraction with toluene was compared to the mass before extraction to determine the gel fraction. Thermal degradation profile of sulfonated SBS was further characterized by thermogravimetric analysis (TGA) using a TA Instruments Discovery Series TGA 550, which were performed under a nitrogen environment to 800 °C at a rate of 20 °C/min. Differential scanning calorimetry (DSC) was carried out with a TA Instruments Discovery Series DSC 250. A heat-cool-heat cycle was used from 0 °C to 200°C with heating rates of 10 °C/min and cooling rates of 5 °C/min. Nitrogen physisorption isotherms of OMC samples (at 77 K) were characterized on a Micromeritics Tristar II 3020. Surface areas of OMC samples were determined through Brunauer–Emmett–Teller (BET) analysis and pore size distributions (PSDs) were determined from nonlocal density functional theory (NLDFT) models. A Zeiss Ultra 60 field-emission scanning electron microscopy (SEM) was employed to characterize the mesoporous structure with an accelerating voltage of 15 kV. From these SEM images, pore size analysis was performed using ImageJ software. Small-angle X-ray scattering (SAXS) was performed on a Xeuss 2.0 laboratory beamline (Xenocs Inc.) with a sample to detector distance of 3.86 m. A copper source was used to irradiate the samples with 8.05 keV X-rays. The Irena and Nika package in Igor Pro (Wavemetrics) software was used for data processing. Domain spacing, d, was determined as $d = 2\pi/q^*$, where q^* is the position of the primary ordering peak. An ESCALAB Xi^+ spectrometer (Thermo Fisher) equipped with a monochromatic Al X-ray source (1486.6 eV) and a MAGCIS Ar^+/Arn^+ gas cluster ion sputter gun was used for X-ray photoelectron spectroscopy (XPS) characterization. A base pressure in the analysis chamber of 3×10^{-7} mbar and a takeoff angle of 90° from the surface was set for spectral acquisition. Spectral analysis was carried out using Avantage software from Thermo Fisher.

Results and Discussion

The sulfonation-induced crosslinking of SBS samples and their further conversion to produce OMCs are schematically illustrated in Figure 1. Briefly, SBS used in this work can self-assemble into ordered cylindrical nanostructures that serve as the starting precursor materials. The polymer crosslinking is performed through submerging SBS pellets in concentrated sulfuric acid for extended periods of time at elevated temperatures. During the sulfonation process, the acid can diffuse through and react with both polystyrene (PS) and PB segments, forming crosslinked networks while maintaining an ordered nanostructure. Subsequently, sulfonation-induced crosslinking can enable the successful conversion of PB segments to carbon upon exposure to high temperatures (>600 °C) in an inert atmosphere. This process is simple and scalable, only involving two processing steps and using low cost, commercially available materials.

Two different reaction temperatures are employed in this work to investigate their impact on reaction kinetics and tunability of the OMCs material properties. The progress of the

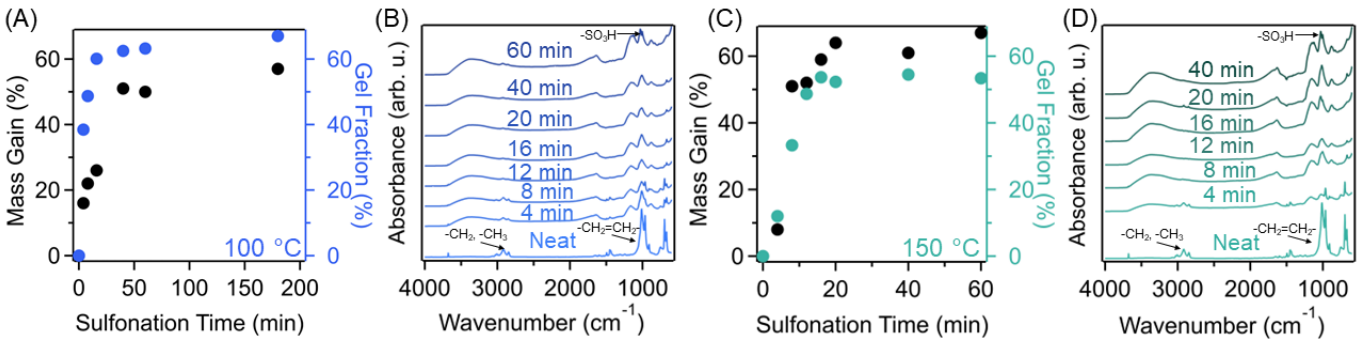

Figure 2. (A) Mass gain and gel fraction and (B) FTIR spectra of SBS reacted at 100 °C as a function of reaction time. (C) Mass gain and gel fraction and (D) FTIR spectra of SBS reacted at 150 °C as a function of reaction time.

sulfonation reaction can be monitored through studying mass gain, gel fraction, and the evolution of functional groups in the polymer through Fourier transform infrared (FTIR) spectroscopy, the results of which are provided in Figure 2. Sulfonating SBS at 100 °C results in gradual increases in both mass gain and gel fraction which begin to plateau around 60 min of reaction at 50 wt% and 62 wt%, respectively. In comparison, the mass gain and gel fraction increase much more rapidly under reaction at 150 °C, where the values begin to plateau after 20 min indicating enhanced reaction kinetics at elevated temperatures. These results are further supported through FTIR spectra provided in Figure 2(B,D). Generally, the progress of the reaction can be monitored through multiple characteristics bands within the spectra. The alkyl stretching vibrations (3130 cm^{-1} – 2824 cm^{-1}), which correspond to reactive sites along the polymer backbone, diminish as the reaction occurs. Similarly, the strong IR band at around 1013 cm^{-1} in the spectrum of neat sample is associated with the alkenes present within the PB units of the polymer. These functional groups are reacted during the crosslinking reaction and the intensity of associated band reduces greatly after reacting at 100 °C and 150 °C for 8 min and 4 min, respectively. A band at 1009 cm^{-1} can be found for both reaction conditions, which is associated with the in-plane skeletal vibrations of aromatic rings in the PS repeat units that are substituted with sulfonic acids. As the reaction progresses, a secondary band at 1030 cm^{-1} evolves, which is representative of increased sulfonation degree of the PB backbone. Similar to the mass gain and gel fraction results, reaction at 150 °C results in more rapid evolution of the chemical structure, indicating faster reaction kinetics. Importantly, the SBS precursor exhibits greatly enhanced crosslinking kinetics than SEBS used in previous work, even at significantly lower reaction temperatures. SEBS required 4 h of reaction at 150 °C to achieve a fully crosslinked state, confirmed by mass gain, gel fraction, and FTIR results.[26] The enhanced sulfonation-induced crosslinking reaction kinetics of the SBS precursors can be attributed to the presence of alkenes within their backbones. These functionalities can readily react to form intermolecular crosslinks, as double bonds are known to be more reactive than single bonds due to their more electron rich nature, which can also facilitate the installation of sulfonic acid groups along the polymer backbone. In turn, diffusion of the concentrated sulfuric acid crosslinking agent is also greatly encouraged resulting in a more rapid reaction. Notably, sulfonation induced crosslinking in polyolefin systems has been demonstrated as a diffusion-controlled reaction.[29–31] Herein, by including unsaturated bonds in the precursor design of the amorphous polyolefin-containing systems (Figure S1), it is found that the required crosslinking time can be significantly reduced from 4 h (for SEBS) to 20 min (for SBS), corresponding to nearly 8-fold enhancement in reaction kinetics.

As discussed earlier, the PS minority phase in SBS is also sulfonated during the crosslinking reaction, which sulfonic acid groups can be installed to the aromatic ring of the PS repeat units.[32] While sulfonation of the PS rings can lead to intermolecular sulfone bridges, the minority PS phase does not contribute to the formation of carbon in the final product, which has been demonstrated in other sulfone-bridged aromatic polymers.[33,34] However, the sulfonation of PS could play an important role in determining the nanostructures of the crosslinked SBS domains, and their derived pores in the OMC after carbonization. For example, sulfonation induced-crosslinking of SEBS leads to an expanded domain spacing from 25.5 nm to 38.0 nm with a reduced degree of ordering, which can be attributed to the competition between nanostructure rearrangement/ordering and crosslinking-induced hindered chain mobility. Moreover, a previous work has demonstrated that while sulfonation poly(styrene)-*block*-poly(isoprene)-*block*-poly(styrene) (SIS) can proceed vigorously,[28] the intense reaction can result in rapid release of gaseous byproducts and strongly disrupt the ordered nanostructure of the BCP precursor. Therefore, it is important to assess how the sulfonation reaction impacts the nanostructure development of SBS materials. Here, we found that crosslinking of SBS results in a reduced degree of ordering of polymer nanostructure, which was confirmed by small angle x-ray scattering (SAXS) measurements as shown in Figure 3. Specifically, the SAXS results of the neat SBS polymer demonstrates ordered structures with domain spacings of 34.2 nm and a full-width at half-maximum (FWHM) of 0.0385 nm^{-1}. However, sulfonation at 100 °C results in a broad primary peak (FWHM: 0.0661 nm^{-1}) which represents a domain spacing of 33.7 nm. Similarly, the sample sulfonated at 150 °C exhibits a broad peak associated with a slightly higher degree of ordering in the system (FWHM: 0.0619 nm^{-1}) compared to their counterparts at 100 °C, and a domain spacing of 33.4 nm. Interestingly, sulfonation of SBS leads to a reduced d-spacing, compared to neat sample, which is contrary to the phenomena observed in the sulfonation of SEBS polymers. We attribute this difference to the rapid kinetics of the crosslinking reaction which can immediately trap the nanostructure prior to their rearrangement toward thermo-equilibrium states. Therefore, the PS domain expansion was almost completely hindered. Subsequently, the network formation from linear polymer chains can leads to a slightly reduced domain spacing due to more densified chain packing, as suggested by many previous studies.[35,36] Additionally, the crosslinking of the polyolefin domains overall results in reduced

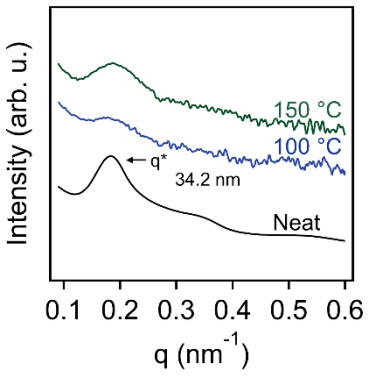

Figure 3. SAXS results for neat SBS in comparison to samples sulfonated at 100 °C for 60 min and 150 °C for 20 min, respectively.

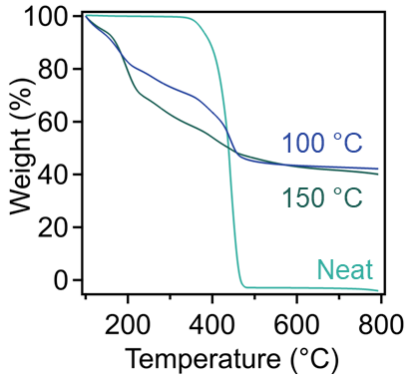

Figure 4. TGA thermogram of neat SBS, SBS sulfonated at 100 °C for 60 min, and SBS sulfonated at 150 °C for 20 min.

ordering in the BCP nanostructures, which is consistent with the broadening of the primary peak in the SAXS patterns of the crosslinked polymers.

The sulfonation induced-crosslinked SBS is converted to carbon through exposure to 800 °C under a N_2 atmosphere. During this process, the minority PS domains thermally decompose to form pores due to the selective crosslinking reaction only occurring within the polyolefin majority phase. Additionally, the sulfonated PB matrix can be converted to carbon upon pyrolysis; this step may result in the loss of functional groups. Thermogravimetric analysis (TGA) was used to study the decomposition of the SBS precursors and their carbon yield (Figure 4). The TGA results indicate carbon yields of 42 wt% and 40 wt% for the samples which were sulfonated at 100 °C for 60 min and 150 °C for 20 min respectively. This result suggests that both sulfonation temperatures can lead to similar carbon yield, while less reaction time is required for the higher reaction temperature. Specifically, Figure 5 shows carbon yield of SBS precursors as a function of crosslinking time at both reaction temperatures, in which a steady increase can be observed until reaching a plateau value. This plateau begins at 60 min for the 100 °C reaction and 20 min for the 150 °C reaction, corresponding well with times required to reach a fully crosslinked state as shown in Figure 1. Additionally, the necessary crosslinking reaction time leading to ordered nanostructures, determined through nitrogen physisorption experiments after carbonization, is illustrated in Figure 5. Specifically, nitrogen physisorption isotherms and their corresponding pore size distributions calculated through nonlocal density functional theory (NLDFT) for carbonized samples that were crosslinked at each time point are presented in Figure S2 for 100 °C and Figure S3 for the 150 °C reaction condition. Despite exhibiting significant carbon yield with shorter reaction times at 100 °C, physisorption isotherms (Figure S2(A,C,E) of the carbonized samples indicate very low Brunauer Emmett Teller (BET) surface areas (<40 m^2/g) indicating a lack of retention of any pore structure. This is further evidenced by their profile of pore size distributions (Figure S2(B,D,F) which only indicate a broad distribution of disordered pores. However, after sufficient crosslinking times have been achieved (>60 min), ordered mesostructures in final carbon products can be achieved, which will be discussed further in the following section. The samples reacted at 150 °C exhibit a similar trend, although order is established in the nanostructure much more rapidly. After 8 min (Figure S3(A,B), the carbonized sample exhibits a BET surface area of 29 m^2/g with a broad pore size distribution, indicating the collapse of the pore structure during carbonization due to insufficient crosslinking. After 12 min of reaction (Figure S3(C,D)), the BET surface area increases to 148 m^2/g, although the pore size distribution of carbon indicates the morphology is still largely disordered. The onset of ordered nanostructures is first exhibited by the carbonized sample that was crosslinked for 16 minutes at 150 °C which exhibits a uniform population of pores with an average width of 9.1 nm and a surface area of 176 m^2/g. While this reaction time was sufficient to produce ordered pore sizes, the surface area is reduced in comparison to samples reacted for longer times, possibly due to local fluctuations in the reaction progress resulting in degradation of portions of the sample that were under-crosslinked; in Figure 5 it also shows that this sample (crosslinked at 150 °C for 16 min) has a low carbon yield (~ 30wt%). Samples crosslinked for longer times

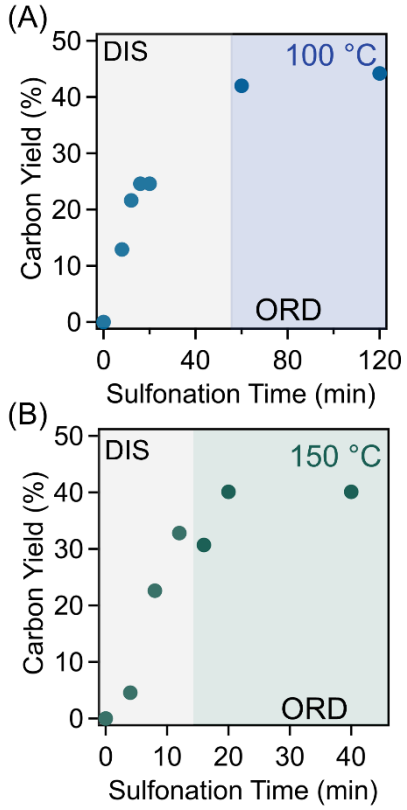

Figure 5. Carbon yield as a function of sulfonation time for samples sulfonated at (A) 100 °C and (B) 150 °C. Gray shading represents datapoints which do not exhibit ordered pores, while the colored shading represents datapoints which were successfully converted to OMCs.

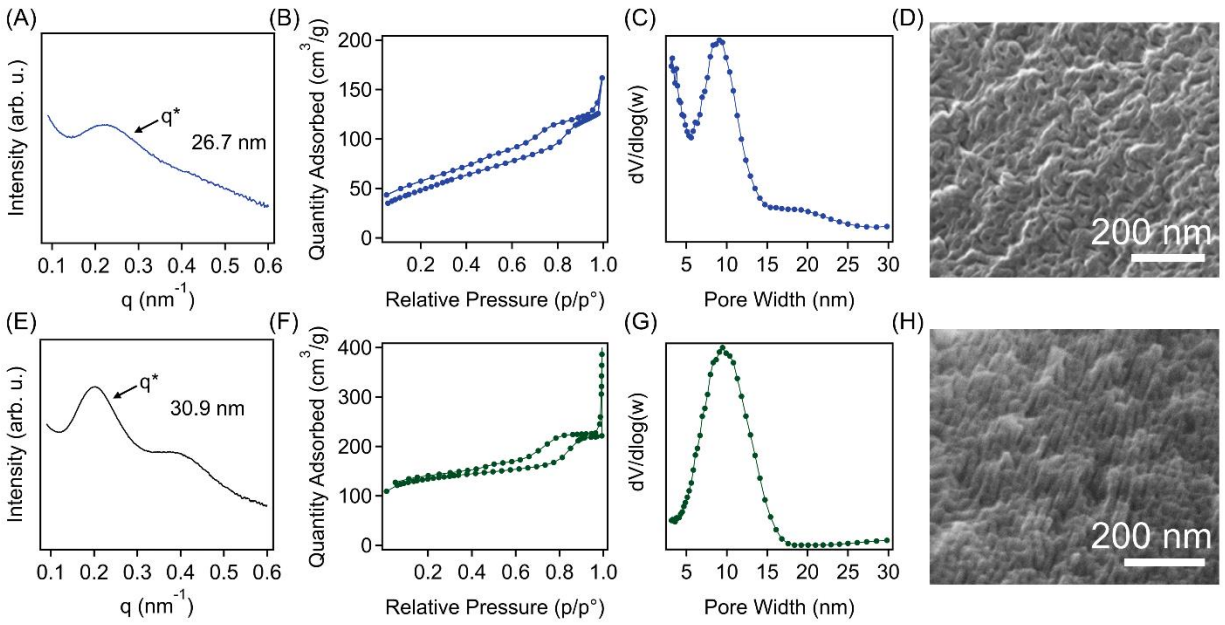

Figure 6. (A) SAXS pattern, (B) nitrogen physisorption isotherm, (C) NLDFT calculated pore size distribution, and (D) SEM image of the SBS100. (E) SAXS pattern, (F) nitrogen physisorption isotherm, (G) NLDFT calculated pore size distribution and (H) SEM image of the SBS150.

will be discussed in the following section. Overall, it was found that 60 min and 20 min are optimal conditions for sulfonation reaction at 100 °C and 150 °C, respectively. These reaction times enable the production of OMCs with maximum carbon yields and ordered structures, while longer reaction times only produce materials with similar carbon yield and pore characteristics (100 °C: Figure S2(E,F); 150 °C: Figure S3(E,F). These conditions were employed for further study, and samples will be referred to as SBS100 and SBS150 throughout the remainder of the discussion, which 100 and 150 represented their crosslinking temperature.

The structure of the SBS-derived OMCs after carbonization were studied through a suite of characterization measurements, including SAXS, physisorption, and SEM, which are all shown in Figure 6. Figure 6(A,E) depict SAXS patterns of the carbonized samples which were crosslinked at 100 °C and 150 °C, respectively. OMC100 has limited degree of ordering in its nanostructure, evidenced by a broad, primary scattering peak, with a domain spacing of 26.7 nm. In comparison, the 150 °C crosslinking temperature resulted in materials that were more ordered with larger domain spacings (30.9 nm). These domain spacings represent a shrinkage from the crosslinked to carbonized state of 20% (100 °C sulfonation) and 7% (150 °C sulfonation). Furthermore, SBS150 sample exhibits long-range ordering which is evidenced by the presence of a secondary peak that is a convolution of two peaks at q*:$\sqrt{3}$ and q*:$\sqrt{4}$ which may suggest a cylindrical morphology, although it is not well-defined. Note that the sharper primary ordering peaks developed in carbonized samples, compared to sulfonated counterparts, is most likely associated with improved X-ray scattering contrast between carbon and air (i.e. pores) in OMCs. After crosslinking, the ordering of nanostructures should not be further developed. The increased shrinkage and disorder in the lower reaction temperature is potentially caused by a slightly reduced degree of crosslinking, which is further evidenced through characterizing the pore textures of these materials. Specifically, nitrogen physisorption experiments were employed to investigate the surface area, porosity, and pore size distributions (PSDs) of the SBS-derived OMCs synthesized with reaction temperatures of 100°C and 150 °C, respectively. Both samples exhibit a typical Type IV isotherm representative of mesoporous materials (Figure 6(B,F), which were further analyzed to understand the pore characteristics of the materials. The BET surface areas of SBS100 and SBS150 were 176 m^2/g and 373 m^2/g, respectively. The reduced surface area of the SBS100 sample is potentially due to a higher degree of loss in ordering upon carbonization. Notably, SBS150 has a comparable surface area to SEBS-derived OMCs demonstrated previously and is also close to some PAN-derived mesoporous carbon systems. For instance, Liu et al. used poly(methyl methacrylate-*block*-polyacrylonitrile block copolymers to fabricate mesoporous carbon fibers through the decomposition of minority poly(methyl methacrylate) phases. The resulting surface area was as high as 503 m^2/g with pore size distributions averaged around 9.3 nm.[19] NLDFT models were used to determine the PSD of the SBS derived-OMCs (Figure 5(C,G)). Both materials exhibited a very similar averaged pore size of 9.1 nm and 9.5 nm for SBS100 and SBS150, respectively. Despite the difference in the SAXS patterns of the carbonized materials from employing different crosslinking conditions, their pore size distribution profiles are similar. This suggests that the lower degree of crosslinking in SBS100 results in contraction of the majority phases during carbonization, eventually leading to thinner pore walls than the SBS150 sample. It is also worth noting that SBS100 demonstrates a shoulder at smaller pore sizes indicating a loss of ordering, which could very likely occur during the carbonization process. Moreover, the SBS150 sample demonstrates a much narrower pore size distribution,

consistent with their SAXS pattern in Figure 6(E), indicating the enhanced degree of ordering, which may be due to the improved structural integrity during the carbonization step. Notably, these samples were carbonized with a ramp rate of 1 °C/min, which resulted in the preservation of the nanostructure of the porous material. Figure S4 depicts the effects of increased carbonization ramp rates (3 °C/min and 10 °C/min) on the pore texture of the carbons. The physisorption measurements indicate a nearly complete collapse of the porous structures evidenced by very low surface areas (8 m^2/g and 19 m^2/g, respectively) which could be a result of the more rapid conversion from polymer to carbons, significantly disrupting the nanostructure and suggesting mechanical integrity of crosslinked polyolefin framework is limited. Furthermore, broad pore size distributions suggest remaining mesopores are largely disordered. SBS-derived carbons fabricated through optimized conditions exhibit pores that are much larger than conventional soft-templated OMCs using common Pluronic surfactants, which are typically 3-6 nm in pore width.[13,37,38] Expanded pore size in OMC materials can be advantageous for applications which involve large-size guest molecules transport and sorption.[14,22,39] Furthermore, scanning electron microscopy (SEM) images (Figure 6 (D,H)) confirm the presence of mesopores in both SBS100 and SBS150 generated from the decomposition of the PS minority phase. Image analysis was performed using ImageJ software to provide further support of the pore sizes fabricated through this process. From the SEM image of SBS100, the average pore size was 10.4 ± 2.5 nm, while SBS150 exhibited an average pore size of 10.0 ± 1.9 nm. The average pore sizes, as well as the long-range ordering in SBS150 sample from SEM imaging are in good agreement with results from nitrogen physisorption and SAXS experiments.

Moreover, an important feature of the sulfonation-induced crosslinking reaction for enabling the SBS-to-OMC conversion is the incorporation of sulfur heteroatoms into the carbon framework. The presence of heteroatoms including nitrogen, phosphorus, boron, and sulfur have been demonstrated to greatly enhance the properties of carbon materials[1,40,41]. In turn, OMC doping amplifies their performance and utility in a number of applications including materials for energy storage,[42,43] catalysis,[44,45] and CO_2 capture.[46,47] For example, sulfur-doping can enhance the OMC performance for oxygen reduction reactions through the addition of positively charged sites into the carbon matrix which can favorably interact with O_2 molecules.[48,49] X-ray photoelectron spectroscopy (XPS) results confirms the successful incorporation of sulfur heteroatoms into the carbon framework of the SBS-derived OMCs. Specifically, XPS survey scans in Figure 7(A,B) depict sulfur contents of 0.6 at% and 1.4 at% for SBS100 and SBS150 samples, respectively, which are in a similar range compared to SEBS-derived OMCs,[26] as well as other functional carbon materials derived from semi-crystalline polyolefin precursors, including polypropylene and polyethylene.[50,51] The level of sulfur content at 1.4 at% is close to other reports of synthesizing sulfur-doped OMCs through the use of dopants, such as benzyl disulfide,[52] thiophenol,[53] sulfur powders.[54,55] Gratifyingly, our systems does not require an additional step of dopant impregnation for incorporation of sulfur heteroatoms in OMC framework. Furthermore, high resolution *S2p* scans in Figure 7(b) indicate the presence of two different bonding environments of sulfur heteroatoms in carbon frameworks, and interestingly, their relative content can be varied by controlling the crosslinking temperature of SBS. Specifically, SBS150 contains a larger ratio of the C-S-O bonds (77 at%) than SBS100 (38 at%). This demonstrates that the reaction condition of sulfonation-induced crosslinking provides additional handles for tuning the material properties for desired applications. For instance, many works have demonstrated that the sulfur doping in the carbon materials can enhance their CO_2 adsorption capacity, and the bonding environment of the heteroatom in the carbon matrix plays a critical role.[56–58] Specifically, C-S-O bonds in sulfur doped carbons provide active sites for the adsorption of CO_2 by tuning the electronic properties of the carbon surface to target the partially positive carbon atom in the CO_2 molecule. The larger populations of the C-S-O bonding environments can result in enhanced CO_2 adsorption capacities. Collectively, SBS 150 exhibits some important advantages over SBS 100, including improved degree of ordering, more rapid reaction kinetics, and higher sulfur heteroatom content with a dominating C-S-O bond type. This work demonstrates that SBS is a low-cost and efficient OMC precursor for preparing large-pore, sulfur-doped due to its fast sulfonation-crosslinking kinetics in concentrated sulfuric acid, while the reaction condition can play a role in determining both the degree of ordering as well as heteroatom content and type in final OMC products.

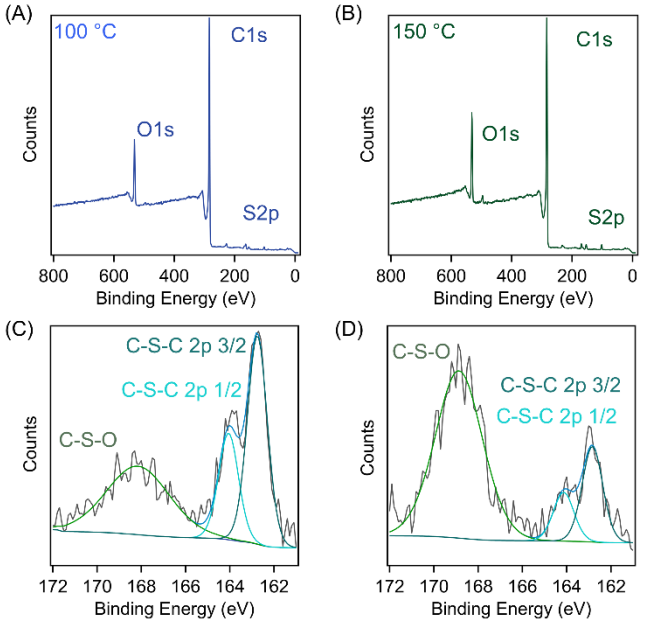

Figure 7. (A,B) XPS survey scans for SBS100 and SBS 150, respectively. (C,D) Corresponding high resolution S2p scans of SBS100 and SBS150, respectively.

Conclusions

Sulfonation-induced crosslinking of polyolefins has been developed for the fabrication of functional carbon materials, which previous efforts were largely focused on carbon fiber

production and waste recycling. In this work, an efficient system for synthesizing OMCs is developed using SBS as the precursor, combined with a two-step process including sulfonation-induced crosslinking and directly pyrolysis. The introduction of unsaturated bonds in precursor backbones enables significantly accelerated crosslinking kinetics, which can be accomplished within 20 min at 150 °C using concentrated sulfuric acid for maximum carbon yield (~ 40 wt%) and relatively high degree of ordering. Resulting OMC materials exhibit ordered mesopores with an averaged pore width of 9-10 nm, which is confirmed by SEM and SAXS measurements. Compared to previous systems, the precursor design in this work enables efficient synthesis of OMCs, which employ low-cost and widely available chemicals, and greatly reduces the processing time and potential energy consumption without sacrificing carbon yield or material properties, such as ordered porous structures. Additionally, changing the fabrication process can selectively alter the doping degree and bonding environments of sulfur heteroatoms within the carbon products, allowing their further tunable functionality toward addressing different targeted applications. Overall, this work presents an efficient and scalable synthesis of OMCs with controllable material properties through precursor and process design.

Author Contributions

M.R. and Z.Q. were responsible for designing experiments during this project. The majority of the experiments were carried out by M.R., A.G. and A.G.O, with assistance from R.D. and A.B. The manuscript was primarily written by M.R. and Z.Q., while all authors contributed. Z.Q. supervised all work through this project.

Conflicts of interest

The authors have submitted a provisional patent that is related to the work presented here.

Acknowledgements

The authors appreciate support from Mississippi SMART Business Act and National Science Foundation (CMMI-2239408). The authors would like to acknowledge Surabhi Jha and Dr. Derek Patton for assistance during XPS experiments, in addition to the NSF (DMR-1726901) which provides funding for acquiring the XPS instrument. The authors would also like to thank Guorong Ma and Yunfei Wang for performing small angle X-ray scattering experiments.

Notes and references

1 Wang, H.; Shao, Y.; Mei, S.; Lu, Y.; Zhang, M.; Sun, J. K.; Matyjaszewski, K.; Antonietti, M.; Yuan, J. *Chem Rev,* 2020, **120**, 9363–9419.
2 Yin, J.; Zhang, W.; Alhebshi, N. A.; Salah, N.; Alshareef, H. N. *Small Methods*, 2020, **4**, 1900853.
3 Pagaduan, J. N.; Samitsu, S.; Varma, J.; Emrick, T.; Katsumata, R. *ACS Appl Polym Mater* 2022, **4**, 4329-4338.
4 Robertson, M.; Zagho, M. M.; Nazarenko, S.; Qiang, Z. *J Polym Sci*, 2022, **60**, 2015-2042.
5 Zu, L.; Zhang, W.; Qu, L.; Liu, L.; Li, W.; Yu, A.; Zhao, D. *Adv Energy Mater*, 2020, **10**, 2002152.
6 Yuan, S.; Gao, Q.; Ke, C.; Zuo, T.; Hou, J.; Zhang, J. *ChemElectroChem*, 2022, **9**, e202101182.
7 Zhang, J.; Zhang, N.; Tack, F. M. G.; Sato, S.; Alessi, D. S.; Oleszczuk, P.; Wang, H.; Wang, X.; Wang, S. *J Hazard Mater*, 2021, **418**, 126266.
8 Gang, D.; Uddin Ahmad, Z.; Lian, Q.; Yao, L.; Zappi, M. E. *Chem Eng J*, 2021, **403**, 126286.
9 Torres, D.; Pérez-Rodríguez, S.; Cesari, L.; Castel, C.; Favre, E.; Fierro, V.; Celzard, A. *Carbon*, 2021, **183**, 12–33.
10 Attia, M. S.; Hassaballah, M. Y.; Abdelqawy, M. A.; Emad-Eldin, M.; Farag, A. K.; Negida, A.; Ghaith, H.; Emam, S. E. *Drug Dev Ind Pharm*, 2021, **47**, 1029–1037.
11 Zhao, Q.; Lin, Y.; Han, N.; Li, X.; Geng, H.; Wang, X.; Cui, Y.; Wang, S. *Drug Deliv.*, 2017, **24**, 94–107.
12 Taguchi, A.; Schüth, F. *Microporous Mesoporous Mater* 2005, **77**, 1–45.
13 Meng, Y.; Gu, D.; Zhang, F.; Shi, Y.; Cheng, L.; Feng, D.; Wu, Z.; Chen, Z.; Wan, Y.; Stein, A.; Zhao, D. *Chem Mater*, 2006, **18**, 4447–4464.
14 Bhardwaj, A.; Pagaduan, J. N.; Yu, Y. G.; Einck, V. J.; Nuguri, S.; Katsumata, R.; Watkins, J. J. *ACS Appl Mater Interfaces*, 2021, **13**, 61027–61038.
15 Zhang, Y.; Qiang, Z.; Vogt, B. D. *RSC Adv*, 2014, **4**, 44858–44867.
16 Kopeć, M.; Lamson, M.; Yuan, R.; Tang, C.; Kruk, M.; Zhong, M.; Matyjaszewski, K.; Kowalewski, T. *Prog Polym Sci*, 2019, **92**, 89–134.
17 Tang, C.; Tracz, A.; Kruk, M.; Zhang, R.; Smilgies, D. M.; Matyjaszewski, K.; Kowalewski, T. *J Am Chem Soc*, 2005, **127**, 6918–6919.
18 Zhong, M.; Kim, E. K.; Mcgann, J. P.; Chun, S.-E.; Whitacre, J. F.; Jaroniec, M.; Matyjaszewski, K.; Kowalewski, T. *J Am Chem* Soc, 2012, **134**, 14846-14857.
19 Zhou, Z.; Liu, T.; Khan, A. U.; Liu, G. *Sci Adv*, 2019, **5**. eaau6852
20 Song, Y.; Wei, G.; Maciej, ‖; Kopeć, K.; Rao, L.; Zhang, Z.; Gottlieb, E.; Wang, Z.; Yuan, R.; Ye, G.; Wang, J.; Kowalewski, T.; Matyjaszewski, K. *ACS Appl Nano Mater* 2018, **1**, 2536-2543.
21 Libbrecht, W.; Verberckmoes, A.; Thybaut, J. W.; van der Voort, P.; de Clercq, J. *Carbon*, 2017, **116**, 528–546.
22 Wei, J.; Sun, Z.; Luo, W.; Li, Y.; Elzatahry, A. A.; Al-Enizi, A. M.; Deng, Y.; Zhao, D. *J Am Chem Soc*, 2017, **139**, 1706–1713.
23 Deng, Y.; Wei, J.; Sun, Z.; Zhao, D. *Chem Soc Rev*, 2013, **42**, 4054–4070.
24 Cipriani, E.; Zanetti, M.; Bracco, P.; Brunella, V.; Luda, M. P.; Costa, L. *Polym Degrad Stab*, 2016, **123**, 178–188.
25 Korte, S.; Brandrup, J.; Immergut, E.H., Grulke (Eds.), *Polymer Handbook (fourth ed.),* Wiley Interscience, New York (1999**)**, 59–66.
26 Robertson, M.; Guillen-Obando, A.; Barbour, A.; Smith, P.; Griffin, A.; Qiang, Z. *Nat Commun*, 2023, **14**, 639.
27 Spontak, R. J.; Patel, N. P. *Curr Opin Colloid Interface Sci* 2000, **5**, 333–340.
28 Guillen Obando, A.; Robertson, M.; Smith, P.; Jha, S.; Patton, D. L.; Qiang, Z. *New J Chem,* 2023, **47**, 1318–1327.
29 Younker, J. M.; Saito, T.; Hunt, M. A.; Naskar, A. K.; Beste, A. *J Am Chem Soc*, 2013, **135**, 6130–6141.
30 Robertson, M.; GüIllen Obando, A.; Emery, J.; Qiang, Z., *ACS Omega* 2022, **7**, 12278–12287.
31 Smith, P.; Obando, A. G.; Griffin, A.; Robertson, M.; Bounds, E.; Qiang, Z. *Adv. Mater.*, 2023, 2208029.
32 Coughlin, J. E.; Reisch, A.; Markarian, M. Z.; Schlenoff, J. B., *J Polym Sci,* 2013, **51**, 2416-2424.

33 Di Vona, M. L.; Sgreccia, E.; Licoccia, S.; Alberti, G.; Tortet, L.; Knauth, P., *J Phys Chem B*, 2009, **113**, 7505-7512.
34 Di Vona, M. L.; Marani, D.; D'Ottavi, C.; Trombetta, M.; Traversa, E.; Beurroies, I.; Knauth, P.; Licoccia, S. *Chem Mater*, 2006, **18**, 69–75.
35 Ishibashi, J. S. A.; Pierce, I. C.; Chang, A. B.; Zografos, A.; El-Zaatari, B. M.; Fang, Y.; Weigand, S. J.; Bates, F. S.; Kalow, J. A. *Macromolecules*, 2021, **54**, 3972–3986.
36 Fang, H.; Gao, X.; Zhang, F.; Zhou, W.; Qi, G.; Song, K.; Cheng, S.; Ding, Y.; Winter, H. H. *Macromolecules*, 2022, **55**, 10900–10911.
37 Qiang, Z.; Guo, Y.; Liu, H.; Cheng, S. Z. D.; Cakmak, M.; Cavicchi, K. A.; Vogt, B. D. *ACS Appl Mater Interfaces*, 2015, **7**, 4306–4310.
38 Wang, J.; Xue, C.; Lv, Y.; Zhang, F.; Tu, B.; Zhao, D. *Carbon*, 2011, **49**, 4580–4588.
39 Liu, C.; Yu, M.; Li, Y.; Li, J.; Wang, J.; Yu, C.; Wang, L. *Nanoscale*, 2015, **7**, 11580–11590.
40 Qiang, Z.; Xia, Y.; Xia, X.; Vogt, B. D. *Chem Mater*, 2017, **29**, 10178–10186.
41 Gao, Y.; Wang, Q.; Ji, G.; Li, A.; Niu, J., *RSC Adv* 2021, **11**, 5361-5383.
42 Song, W.; Kan, J.; Wang, H.; Zhao, X.; Zheng, Y.; Zhang, H.; Tao, L.; Huang, M.; Liu, W.; Shi, J. *ACS Appl Nano Mater*, 2019, **2**, 5643–5654.
43 Qiang, Z.; Chen, Y. M.; Gurkan, B.; Guo, Y.; Cakmak, M.; Cavicchi, K. A.; Zhu, Y.; Vogt, B. D. *Carbon*, 2017, **116**, 286–293.
44 Jiang, T.; Wang, Y.; Wang, K.; Liang, Y.; Wu, D.; Tsiakaras, P.; Song, S. *Appl Catal B*, 2016, **189**, 1–11.
45 Wang, Y.; Liu, M.; Zhao, X.; Cao, D.; Guo, T.; Yang, B. *Carbon*, 2018, **135**, 238–247.
46 Robertson, M.; Obando, A. G.; Nunez, B.; Chen, H.; Qiang, Z. *ACS Appl. Eng. Mater*, 2022, **2023**, 165–174.
47 Liu, X.; Zhou, Y.; Wang, C. L.; Liu, Y.; Tao, D. J. *Chem Eng J*, 2022, **427**, 130878.
48 Liang, J.; Jiao, Y.; Jaroniec, M.; Zhang Qiao, S. *Angew Chem Int Ed,* 2012, **51**, 11496-11500
49 Yang, Z.; Yao, Z.; Li, G.; Fang, G.; Nie, H.; Liu, Z.; Zhou, X.; Chen, X; Huang, S. *ACS Nano*, 2012, **6**, 205-211.
50 Lee, G.; Eui Lee, M.; Kim, S. S.; Joh, H. I.; Lee, S. *J Ind Eng Chem*, 2022, **105**, 268–277.
51 Yang, I.; Mok, J. H.; Jung, M.; Yoo, J.; Kim, M. S.; Choi, D.; Jung, J. C. *Macromol Rapid Commun*, 2022, **43**, 2200006.
52 Wang, H.; Bo, X.; Zhang, Y.; Guo, L. *Electrochim Acta*, 2013, **108**, 404–411.
53 Maluta, J. R.; Machado, S. A. S.; Chaudhary, U.; Manzano, J. S.; Kubota, L. T.; Slowing, I. I. *Sens Actuators B Chem*, 2018, **257**, 347–353.
54 Li, Z.; Cao, Y.; Li, G.; Chen, L.; Xu, W.; Zhou, M.; He, B.; Wang, W.; Hou, Z. *Electrochim Acta*, 2021, **366**, 137466.
55 Sun, H.; Li, G.; Xu, A.; Xu, Z.; Wu, S. *J Alloys Compd*, 2022, **906**, 164311.
56 Seredych, M.; Jagiello, J.; Bandosz, T. J. *Carbon N Y*, 2014, **74**, 207–217.
57 Cui, H.; Xu, J.; Shi, J.; Zhang, C. *J CO2 Util*, 2021, **50**, 101582.
58 Shi, J.; Yan, N.; Cui, H.; Liu, Y.; Weng, Y. *J Environ Chem Eng*, 2017, **5**, 4605–4611.